



**HAL**  
open science

# Alternative determinism principle for topological analysis of chaos

Marc Lefranc

► **To cite this version:**

Marc Lefranc. Alternative determinism principle for topological analysis of chaos. 2005. hal-00004359v2

**HAL Id: hal-00004359**

**<https://hal.science/hal-00004359v2>**

Preprint submitted on 19 May 2005 (v2), last revised 31 Aug 2006 (v3)

**HAL** is a multi-disciplinary open access archive for the deposit and dissemination of scientific research documents, whether they are published or not. The documents may come from teaching and research institutions in France or abroad, or from public or private research centers.

L'archive ouverte pluridisciplinaire **HAL**, est destinée au dépôt et à la diffusion de documents scientifiques de niveau recherche, publiés ou non, émanant des établissements d'enseignement et de recherche français ou étrangers, des laboratoires publics ou privés.

# **Alternative determinism principle for topological analysis of chaos**

Marc Lefranc

*Laboratoire de Physique des Lasers, Atomes, Molécules, UMR CNRS 8523,*

*Centre d'Études et de Recherches Lasers et Applications,*

*Université des Sciences et Technologies de Lille, F-59655 Villeneuve d'Ascq, France*

(Dated: May 19, 2005)

## **Abstract**

The topological analysis of deterministic chaos based on a knot-theoretic characterization of unstable periodic orbits has proved a powerful method, however knot theory can only be applied to three-dimensional systems. Still, the core principles upon which this approach is built, determinism and continuity, apply in any dimension. We propose an alternative framework in which these principles are enforced on triangulated surfaces rather than curves. As a first step toward a formalism applicable in higher dimensions, we show that in dimension three our approach predicts the correct topological entropies for periodic orbits of the horseshoe map.

PACS numbers: 05.45.-a

ccsd-00004359, version 2 - 19 May 2005

A dynamical system is naturally described as a flow connecting states to other states in a phase space. Chaotic behavior occurs when trajectories become unstable to perturbations, and results from the interplay of two geometrical processes: *stretching* separates neighboring trajectories exponentially fast while *squeezing* maintains the flow within a bounded region [1, 2, 3]. A topological analysis has been developed to classify the ways in which the stretching and squeezing mechanisms can organize a chaotic attractor [2, 3, 4, 5]. It relies on a theorem stating that unstable periodic orbits (UPO) of a chaotic three-dimensional (3D) flow can be projected onto a 2D branched manifold (a *template*) without modifying their knot invariants [6]. This property has been harnessed to design an analysis of experimental time series [4, 5] that seeks to determine the simplest template compatible with the topological invariants of UPO extracted from the time series [2, 3].

Although the relevance of this approach has been confirmed in several experiments [2, 3, 5], it can only be applied to 3D attractors: in higher dimensions, all knots can be deformed into each other. A first step to overcome this limitation is to recognize that knot theory is not a core ingredient of topological analysis but simply a convenient way to study how two fundamental properties, determinism and continuity, constrain trajectories in phase space. It is because two trajectories cannot intersect that the knot type of a 3D periodic orbit is well defined and that it is not modified as the orbit is deformed under control parameter variation. Thus, we need to build a framework where UPO are characterized by mathematical objects playing the same role in any phase space dimension as knot invariants in dimension three, i.e., that can classify periodic orbits according to whether they can be deformed into each other without violating determinism and continuity.

In this paper, we propose a formalism which enforces the non-intersection requirement on objects whose dimension varies with that of phase space, yet remains applicable to UPO extracted from experimental signals. It is based on a representation of the dynamics in a triangulated space whose nodes are periodic points in a Poincaré section. In dimension three, its explicit construction is easy, and we find that the new formalism predicts the correct topological entropies for periodic orbits of the horseshoe map. This is an important result because a positive-entropy orbit is a powerful indicator of chaos [5, 7]; it suggests that we have captured a key ingredient for constructing a knotless topological analysis. However, all the details of the higher-dimensional theory are not yet understood, and we postpone its description to a future work.

We now detail our approach. A first step is to replace the requirement of non-intersecting

curves by a geometrical problem that adapts naturally to phase spaces of any dimension. It has been suggested to exploit the fact that invariant manifolds of UPO have a rigid structure [5, 8]. In this work, we note that a consequence of determinism is that as a volume element  $V$  of a  $d$ -dimensional phase space is advected by a chaotic flow  $\Phi_t$ , the image  $\Phi_t(\partial V)$  of its boundary, although stretched and squeezed, cannot display self-intersections: at any time  $t$ , its interior and its exterior remain distinct, as with a droplet in a fluid flow. A technical formulation of this property is that volume orientation is preserved by the dynamics.

For the sake of simplicity, we restrict ourselves to attractors embedded in  $\mathbb{R}^n \times S^1$  (e.g., forced systems), that can be sliced into  $n$ -dimensional Poincaré sections parameterized by  $\varphi \in S^1$ . The non-intersection theorem can then be applied to boundaries of  $n$ -dimensional volume elements of Poincaré sections (Fig. 1). In particular, successive images of a boundary by a first return map should all have the same orientation.

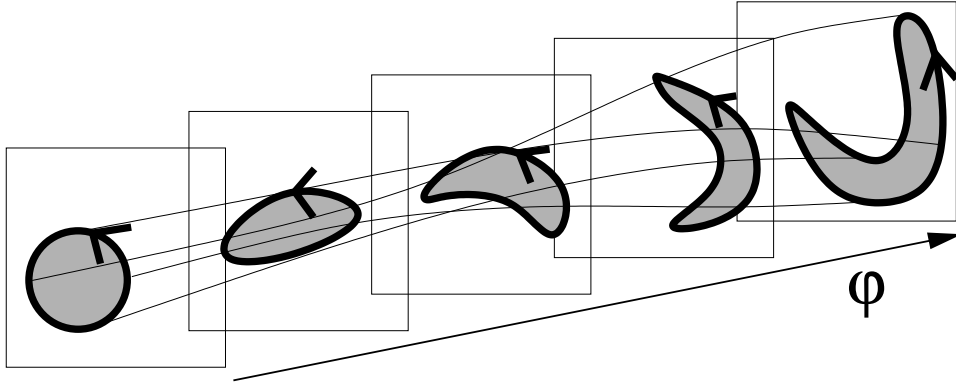


FIG. 1: Under the action of the flow, volume elements of Poincaré sections and their boundaries are stretched and squeezed but retain their orientation, as illustrated here for 2D section planes.

Topological analysis must be applicable to UPO extracted from experimental signals, thus the only piece of data on which it can rely is the trajectory in phase space of a period- $p$  orbit, i.e., the positions in successive Poincaré sections of its  $p$  intersections. From these data, we must obtain information on the evolution of surfaces attached to these periodic points.

To this end, we represent the dynamics in a triangulated space whose nodes are  $p$  periodic points  $P_i$  in a Poincaré section, with  $P_{i+1} = F(P_i)$ ,  $F$  being the return map. In this space, points  $P_i$  are 0-cells, line segments  $\langle P_i, P_j \rangle \equiv \langle ij \rangle$  joining two points are 1-cells, triangles  $\langle P_i, P_j, P_k \rangle \equiv \langle ijk \rangle$  are 2-cells, etc (Fig. 2a). A collection of contiguous  $m$ -cells (e.g., triangles linked through their edges) is the analog in this space of a  $m$ -dimensional surface in the original phase space. We denote by

$S_m$  the set of such collections. Unlike in [9] where similar concepts were used to analyze the static structure of the attractor, we focus here on the dynamics. As Poincaré sections are swept, periodic points move in the section plane and so do the  $m$ -cells attached to them (Fig. 2b). Ideally, the dynamics induced in  $S_m$  should reflect that of  $m$ -dimensional phase-space surfaces under action of the chaotic flow, and in particular be organized by the same stretching and squeezing mechanisms.

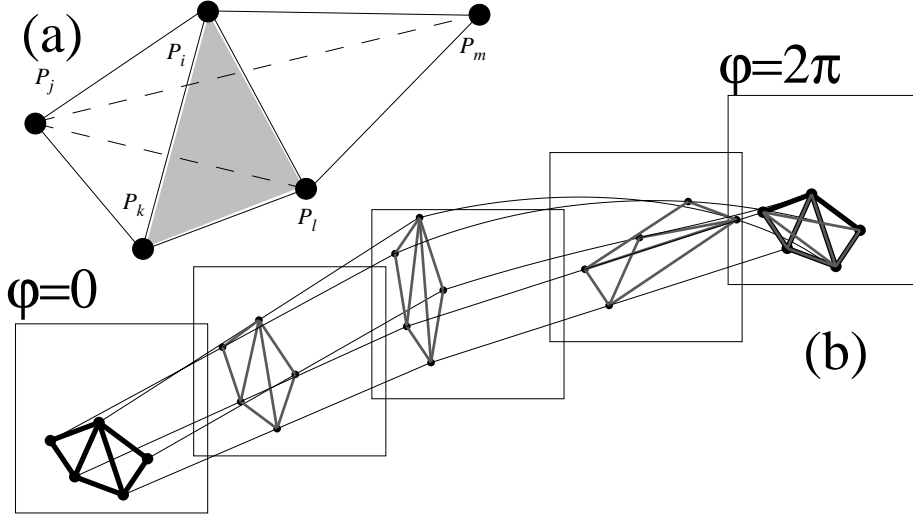


FIG. 2: (a) Triangulated space based on periodic points  $P_i$  in a 3D Poincaré section. The 2-cell  $\langle ikl \rangle$  is shaded. (b) The flow induces a mapping of this triangulated space into itself, as illustrated here for a period-5 orbit embedded in  $\mathbb{R}^2 \times S^1$ .

As illustrated by Fig. 2b, we want to lift dynamical information from  $S_0 = \{P_i\}$  to  $m$ -th order spaces  $S_m$  by constructing a set  $\{F_0, F_1, \dots, F_n\}$  of maps  $F_m : S_m \rightarrow S_m$  that can be viewed as induced by the same Poincaré return map  $F$ . These maps should be continuous, invertible and *satisfy determinism*. Because periodic points are mapped to periodic points under  $F$ , we expect that each  $m$ -cell is mapped under  $F_m$  to another cell or to a set of contiguous cells. Since the volume elements of the triangulated space are the  $n$ -dimensional simplices  $\langle i_1 i_2 \dots i_n i_{n+1} \rangle$ , we focus here on constructing a dynamics  $F_{n-1} : S_{n-1} \rightarrow S_{n-1}$  of their boundaries. As we see below, this can be achieved by keeping track of changes of orientation of  $n$ -dimensional simplices as Poincaré sections are swept.

For clarity, we now specialize to the 3D case. The simplest volume element of a triangulated set of periodic points in a 2D Poincaré section is a triangle (2-cell) based on three periodic points  $P_i, P_j, P_k$ . Denote by  $P_i(\varphi)$  the position of periodic point  $P_i$  in the section plane labeled by  $\varphi$ , with  $P_i(0) = P_i$  and  $P_i(2\pi) = P_{i+1}$ . The simplest description of the evolution of  $T = \langle P_i, P_j, P_k \rangle$  in

successive Poincaré sections is given by

$$T(\varphi) = \langle P_i(\varphi), P_j(\varphi), P_k(\varphi) \rangle. \quad (1)$$

This would lead to a trivial induced return map

$$F_2(T) = T(2\pi) = \langle P_{i+1}, P_{j+1}, P_{k+1} \rangle, \quad (2)$$

if additional rules were not required to enforce determinism and continuity. As long as  $T(\varphi)$  retains its initial orientation, Eq. (1) is adequate. However, it commonly happens that at some time  $\varphi = \varphi_0$ , one of the three points [say  $P_k(\varphi)$ ] passes between the two others, thereby changing the orientation of the triangle  $\langle P_i(\varphi), P_j(\varphi), P_k(\varphi) \rangle$  (Fig. 3). A naive application of Eq. (1) would then imply that  $T = T(0)$  and  $F_2(T) = T(2\pi)$  have different orientations. As emphasized above, this is strictly forbidden by determinism, and we must thus modify the representation of the dynamics. It turns out that there exists a simple and elegant solution to this problem.

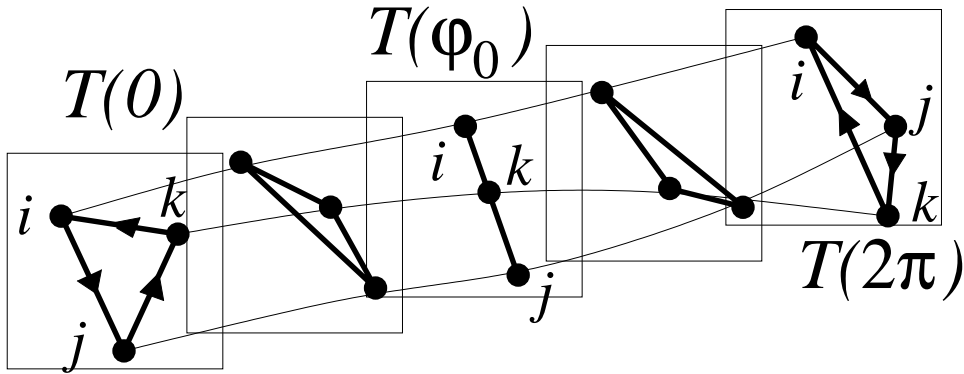


FIG. 3: As three points move in the section plane, the triangle they form can change its orientation.

A degenerate triangle (such as  $T(\varphi_0)$  in Fig. 3) is similar to a flattened balloon whose boundary can be decomposed into two superimposed sides with opposing outer normals. Determinism appears to be violated when these two sides seemingly go through each other so that interior and exterior, as defined with respect with the outer normal, seem to be exchanged. However, only the motion of points is fixed by the experimental data, the dynamics of surfaces is interpolated from this information. Determinism violation can thus result from an incorrect interpretation of point motion. To preserve determinism, we assume that the two opposing sides actually do not cross and enforce this fact in the dynamics by swapping the two sides at the degeneracy, thereby canceling the inversion.

This prescription is illustrated in Fig. 4 where the two opposing sides at triangle degeneracy are represented as a solid and a dashed line, respectively. The key point is that we construct the edge dynamics so that the left (solid line) and right (dashed line) sides remain at the left and right, respectively. Since the left (resp., right) side consists of itinerary  $\langle ik \rangle + \langle kj \rangle$  (resp.,  $\langle ij \rangle$ ) before degeneracy and of itinerary  $\langle ij \rangle$  (resp.  $\langle ik \rangle + \langle kj \rangle$ ) after degeneracy, their relative position is preserved by associating triangle inversion with the following dynamical rule in  $S_1 = S_{n-1}$ :

$$\langle ij \rangle \rightarrow \langle ik \rangle + \langle kj \rangle \quad (3a)$$

$$\langle ik \rangle + \langle kj \rangle \rightarrow \langle ij \rangle \quad (3b)$$

These rules also apply to reverse paths (e.g.,  $\langle ji \rangle \rightarrow \langle jk \rangle + \langle ki \rangle$  follows from (3a)).

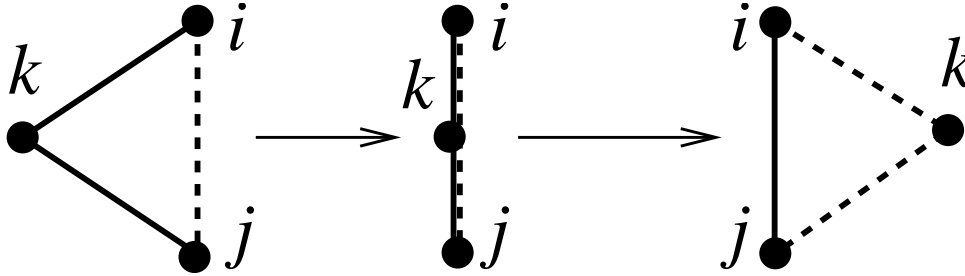


FIG. 4: A triangle is inverted as  $P_k$  passes between  $P_i$  and  $P_j$ . Identifying the solid (resp., dashed) paths in the initial and end configurations leads to substitution (3).

It is easy to check that  $\partial T = \partial \langle ijk \rangle = \langle ij \rangle + (\langle jk \rangle + \langle ki \rangle)$  is mapped to  $(\langle ik \rangle + \langle kj \rangle) + \langle ji \rangle = \partial \langle ikj \rangle$  by (3). This change in point ordering compensates for the change in the triangle orientation so that orientation of  $\partial T$ , and hence determinism, is preserved. Practically, itineraries visiting edges  $e_{ij} = \langle ij \rangle$  in a given order can be viewed as words in a language  $\mathcal{A}^*$  over alphabet  $\mathcal{A} = \{e_{lm}\}$ , and (3) as a substitution operator  $\sigma_{ij}^k$  that in each word  $w$  replaces the letter  $e_{ij}$  by the string  $e_{ik}e_{kj}$  and  $e_{ik}e_{kj}$  by  $e_{ij}$  [hence  $(\sigma_{ij}^k)^2 = 1$ ]. For example,

$$\sigma_{ij}^k e_{kl} e_{li} \overline{e_{ij}} e_{jl} e_{li} \overline{e_{ik}e_{kj}} \overline{e_{ji}} \dots = e_{kl} e_{li} \overline{e_{ik}e_{kj}} e_{jl} e_{li} \overline{e_{ij}} \overline{e_{jk}e_{ki}} \dots$$

The  $\sigma_{ij}^k$  generate a non-trivial dynamics, as the image of an itinerary depends on how periodic points rotate around each other. In spite of its simplicity, this dynamics faithfully reflects that of the flow around the periodic orbit, as we now show by computing the topological entropy of the orbit.

By following the motion of intersections of an orbit  $P$  with consecutive section planes [Fig. 2(b)], we record a list of  $l$  triangle inversions  $\sigma_{i_m j_m}^{k_m}$ . From this list, we build a substitution dynamical system that transforms a word  $w \in \mathcal{A}^*$  into another word according to:

$$F_1 : w \rightarrow w' = N \sigma_{i_1 j_1}^{k_1} \cdots \sigma_{i_l j_l}^{k_l} w, \quad (4)$$

where  $N e_{ij} \cdots = e_{(i+1)(j+1)} \cdots$ . Consider the case of the periodic orbit 00111 of the standard horseshoe map equipped with the usual symbolic coding [2] (Figs. 2b and 5a). We find that the induced return map is  $F_1 = N \sigma_{23}^4 \sigma_{25}^4 \sigma_{13}^4 \sigma_{15}^4$ , leading to the substitution system (we only give asymptotically relevant rules and omit those for reverse paths):

$$e_{14} \rightarrow e_{25}, e_{15} \rightarrow e_{25} e_{51}, e_{25} \rightarrow e_{35} e_{51}, e_{35} \rightarrow e_{41}. \quad (5)$$

Table I displays iterates  $F_1^m(w)$  of  $w = e_{15}$  computed using (5). Their length  $|F_1^m(w)|$  diverges exponentially as  $m \rightarrow \infty$ , indicating that trajectories in the neighborhood of the orbit are continuously stretched apart by the flow. The growth rate:

$$h_T(P) = \lim_{m \rightarrow \infty} \frac{\ln |F_1^m(w)|}{m} \quad (6)$$

should be equal to the topological entropy of the periodic orbit [10], a powerful indicator of chaos [5, 7]. It is obtained as the logarithm of the leading eigenvalue of the incidence matrix  $(M_{ee'})$ , whose entries indicate how many times edge  $e'$  or its reverse edge occurs in  $F_1(e)$ . Here,  $h_T(00111) \sim 0.5435$ .

Table 1 also shows how  $F_1^{kp}(w)$  (where  $p$  is the orbit period) converges towards an infinite word  $w_\infty$  satisfying  $F_1^p(w_\infty) = w_\infty$ . The invariant word  $w_\infty$  is the discrete analog of the infinitely folded unstable manifold of the periodic orbit.

The induced map (5) can be entirely specified by its action on edges  $e_{ij}$ . Because of the ‘‘squeezing’’ rules (3b), this is not always the case. For example, the induced map  $F_1$  for horseshoe orbit 0010111 features the length-decreasing rule  $e_{16} e_{67} \rightarrow e_{17}$ . An incidence matrix then cannot be defined, although entropy estimates can still be obtained by direct iteration. In every example we considered, enlarging the alphabet with special sequences such as  $e_{167} \equiv e_{16} e_{67}$  and then applying suitable recodings always allowed us to rewrite the induced map  $F_1$  as an ordinary substitution like (5). For example, the induced return map characterizing the structure of horseshoe orbit

$m$	Itinerary of $F_1^m(e_{15})$
0	15
1	251
2	35152
3	41525153
4	5251535152514
5	1535152514152515351525
6	2514152515351525251535152514152515351
10	1535152514152515351525251535152525153515...
15	1535152514152515351525251535152525153515...
100	1535152514152515351525251535152525153515...

TABLE I: A few iterates  $F_1^m(e_{15})$  are given by their itinerary between periodic points (e.g., 35152 denotes the path  $e_{35}e_{51}e_{15}e_{52}$ ).

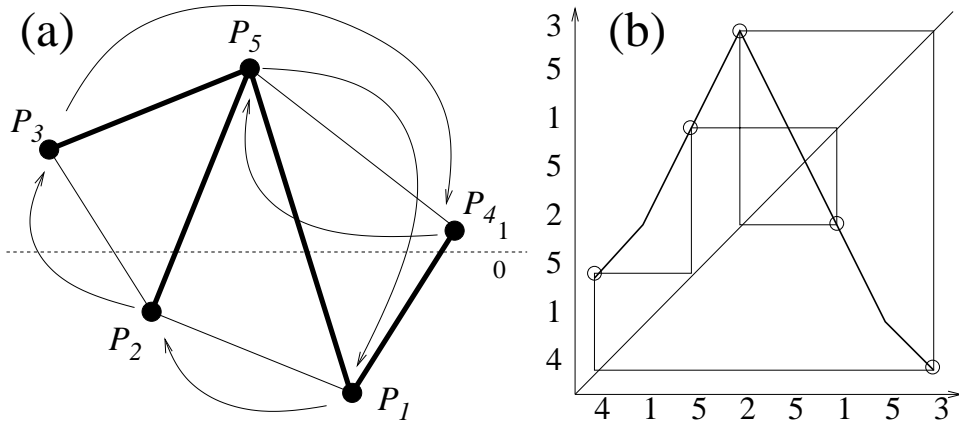


FIG. 5: (a) Periodic points of the horseshoe orbit 00111 and their schematic trajectory in section plane. Bold lines indicate edges involved in the asymptotic dynamics of (5). (b) Path  $P_4P_1P_5P_2P_5P_1P_5P_3$  folds onto itself under action of induced return map  $F_1$ . The unimodal map obtained has 00111 as a periodic orbit.

0010111 can be rewritten as

$$\begin{aligned}
e_{14} &\rightarrow e_{25}, \quad e_{15} \rightarrow e_{257}e_{76}, \quad e_{17} \rightarrow e_{257}e_{71}, \\
e_{25} &\rightarrow e_{37}e_{76}, \quad e_{37} \rightarrow e_{41}, \quad e_{67} \rightarrow e_{71}, \\
e_{167} &\rightarrow e_{25}e_{51}, \quad e_{257} \rightarrow e_{37}e_{761}
\end{aligned} \tag{7}$$

where  $e_{ijk}$  is the letter obtained from the recoding  $e_{ij}e_{jk} \rightarrow e_{ijk}$ . An incidence matrix can then be

Orbit	This work	TTA	Orbit	This work	TTA
01101 $\frac{0}{1}$	0.4421	0.4421	00010 $\frac{0}{1}$	0.3822	0.3822
001011 $\frac{0}{1}$	0.3460	0.3460	000101 $\frac{0}{1}$	0.5686	0.5686
00101 $\frac{0}{1}$	0.4768	0.4768	0001 $\frac{0}{1}$	0.6329	0.6329
001010 $\frac{0}{1}$	0.4980	0.4980	000111 $\frac{0}{1}$	0.5686	0.5686
001 $\frac{0}{1}$	0.5435	0.5435	00011 $\frac{0}{1}$	0.3822	0.3822
001110 $\frac{0}{1}$	0.4980	0.4980	000010 $\frac{0}{1}$	0.4589	0.4589
00111 $\frac{0}{1}$	0.4768	0.4768	00001 $\frac{0}{1}$	0.6662	0.6662
001111 $\frac{0}{1}$	0.3460	0.3460	000011 $\frac{0}{1}$	0.4589	0.4589
001101 $\frac{0}{1}$	0.4980	0.4980	000001 $\frac{0}{1}$	0.6804	0.6804

TABLE II: Topological entropies obtained for positive-entropy horseshoe orbits up to period 8 with the approach described in this work and with the train-track algorithm (TTA) [10, 11, 12].

written for (7), with entropy  $h_T(0010111) \sim 0.4768$ .

For all 746 periodic orbits of the horseshoe map up to period 12, we have compared topological entropies given by our approach and by the train-track algorithm [10, 11], as implemented in the TRAINS computer code [12]. As illustrated in Table II, we found *exact agreement in each instance*. This provides strong evidence that in dimension three, our approach is equivalent to the train track approach. Qualitative properties of chaos are also reproduced: the dynamics is deterministic (by construction), invertible, and the stretching and squeezing processes are described in a completely symmetrical way.

Remarkably, we note that while transformations (4) are *invertible*, the asymptotic dynamics has *underlying singularities*. For example, we consider the itinerary  $w_0 = F^3(e_{15}) = (41525153)$  in Table I, which is the shortest subpath of  $w_\infty$  visiting the four segments involved in (5). As Fig. 5(b) shows, the image  $F_1(w_0) = (5251535152514) = (525153) + (35152514)$  consists of a subpath of  $w_0$  concatenated with a reverse copy of  $w_0$ : *this path is folded onto itself by a one-dimensional map*. The same property holds for all subsequent iterates  $F^m(e_{15})$ , hence for the infinite word  $w_\infty$ . This directly reflects the fact that associated to an invertible return map (e.g., Hénon map), there exists an underlying lower-dimensional noninvertible map (e.g., logistic map) that describes the dynamics restricted to the unstable manifold, a keystone of the Birman-Williams construction [2, 6]. Note that the symbolic name of the orbit can be obtained directly from Fig. 5(b), much more

easily than in [13]. Given the singular return map and layering information obtained by continuity arguments, the simplest template that can carry the periodic orbit studied could then be determined. For the first time, a knotless topological analysis of chaos seems at hand.

That reformulating the determinism principle to make it dimension-independent leads to a more natural formalism in three dimensions suggests that we have captured an essential ingredient for constructing a higher-dimensional topological analysis. Thus we conjecture that in a  $(n + 1)$ -dimensional phase space  $\mathbb{R}^n \times S^1$ , the structure of a periodic orbit can be described by a “braid word” listing successive changes of orientation of simplexes based on  $n + 1$  periodic points as Poincaré sections are swept. Preserving orientation simplex inversions by exchanging sets of facets is expected to induce a non-trivial dynamics in the space of triangulated hypersurfaces.

In conclusion, we have proposed a framework for constructing a topological analysis of higher-dimensional chaos. By recasting the determinism principle in terms of orientation preservation rather than non-intersection of curves and enforcing it in a triangulated space, we have constructed a simple formalism that is equivalent to previous approaches in three dimensions, as demonstrated by entropy calculations. Our preliminary results also suggest that it leads to a faithful combinatorial description of the folding of the invariant unstable manifold over itself, yielding key information about the symbolic dynamics of the orbit. This formalism will naturally extend to higher dimensions once substitution rules associated to different types of simplex inversion are determined. We might then be in a position to classify higher-dimensional chaotic systems, study their symbolic dynamics and their bifurcation sequences. Another important application would be to obtain direct evidence of higher-order singularities (e.g., cusps) in the dynamics along higher-dimensional unstable manifolds [2].

The ideas described here grew out of innumerable discussions with R. Gilmore, to whom I am very much indebted for sharing his insight with me. I thank T. Hall, J. Los and F. Gautero for helpful explanations about the train track algorithm, and M. Nizette, T. Tsankov, J.-C. Garreau, C. Szwaj and S. Bielawski for a careful reading of this manuscript. CERLA is supported by the Ministère chargé de la Recherche, Région Nord-Pas de Calais and FEDER.

---

[1] E. Ott, *Chaos in Dynamical Systems* (Cambridge University Press, Cambridge, 1993).

[2] R. Gilmore and M. Lefranc, *The Topology of Chaos* (Wiley, New York, 2002).

- [3] R. Gilmore, *Rev. Mod. Phys.* **70**, 1455 (1998).
- [4] G. B. Mindlin *et al.*, *Phys. Rev. Lett.* **64**, 2350 (1990).
- [5] G. B. Mindlin *et al.*, *J. Nonlinear Sci.* **1**, 147 (1991).
- [6] J. S. Birman and R. F. Williams, *Topology* **22**, 47 (1983).
- [7] A. Amon and M. Lefranc, *Phys. Rev. Lett.* **92**, 094101 (2004).
- [8] G. B. Mindlin and H. G. Solari, *Physica D* **102**, 177 (1997).
- [9] D. Sciamarella and G. B. Mindlin, *Phys. Rev. Lett.* **82**, 1450 (1999).
- [10] P. Boyland, *Topology Appl.* **58**, 223 (1994).
- [11] M. Bestvina and M. Handel, *Topology* **34**, 109 (1995).
- [12] T. Hall, TRAINS, software available from  
[http://www.liv.ac.uk/math/PURE/MIN\\_SET/CONTENT/members/T\\_Hall.html](http://www.liv.ac.uk/math/PURE/MIN_SET/CONTENT/members/T_Hall.html).
- [13] J. Plumecoq and M. Lefranc, *Physica D* **144**, 231 (2000).